The largest deep-focus Sea of Okhotsk earthquake May 24, 2013, Mw=8.3

Chebrov et al.

Kamchatka Branch of Geophysical Survey of Russian Academy of Sciences (RAS)

Petropavlovsk-Kamchatsky

1

Notable Events

1.1 The largest deep-focus Sea of Okhotsk earthquake May 24, 2013, Mw=8.3

V. N. Chebrov[1] (1949-2016), D. V. Chebrov[1], I. R. Abubakirov[1], A. Yu. Chebrova[1], A. A. Gusev[1&2],
E. M. Guseva[1], D. V. Droznin[1], S. Ya. Droznina[1], E. M. Ivanova[1], N. M. Kravchenko[1],
Yu. A. Kugaenko[1], A. V. Lander[3], E. A. Matveenko[1], S. V. Mitushkina[1], D. A. Ototiuk[1],
V. M. Pavlov[1], A. A. Raevskaya[1], V. A. Saltykov[1], A. A. Skorkina[1], N. N. Titkov[1]

Viktor N. Chebrov (1949-2016)

Danila V. Chebrov

1. Kamchatka Branch of Geophysical Survey of Russian Academy of Sciences (RAS), Petropavlovsk-Kamchatsky

2. Institute of Volcanology and Seismology, RAS, Petropavlovsk-Kamchatsky

3. Institute of Earthquake Prediction Theory and Mathematical Geophysics of RAS, Moscow

1.1.1 Introduction

On May 24, 2013, at 05:44 (UTC) a magnitude Mw 8.3 earthquake occurred in the Sea of Okhotsk, to the west of the Kamchatka Peninsula (Figure 1.1). The scalar seismic moment of the event is $M_0 = 3.95 \cdot 10^{21} N \cdot m$ (*Ekström et al.*, 2012). This is the strongest earthquake recorded in the Kamchatka region during the years of instrumental seismological observations (from 1962 to present) and the most powerful earthquake in the world among events of comparable depths. A similar strong deep-focus event (647 km depth, $M_0 = 2.63 \cdot 10^{21} Nm$) occurred in Bolivia, on June 9, 1994, but this event turned out to be weaker than the Sea of Okhotsk one.

Co-seismic displacement signals of the Sea of Okhotsk earthquake were recorded by many Far Eastern stations of the Global Navigation Satellite System (GNSS) (*Chebrov et al.*, 2013) and the macroseismic effect could be felt globally.

According to KB GS RAS, the epicenter of the May 24, 2013 earthquake is about 360 km north-west of Petropavlovsk-Kamchatsky, the hypocenter is located in the Kamchatka Benioff zone at a depth of 630 km, which corresponds to the lower depth limit for seismic events. The earthquake was followed by an aftershock sequence. Parameters of hypocenters for the earthquake and its strongest aftershocks with $ML \geq 6.0$, energy characteristics according to several seismological agencies of Russia and the world are given in Table 1.1.

Previous strong deep-focus earthquakes in the Sea of Okhotsk area occurred on July 05, 2008 at a depth of 665 km with Mw=7.7 and on November 24, 2008 at a depth of 564 km with Mw=7.3.

The 2013 Sea of Okhotsk earthquake was felt in the Kamchatka region with intensities up to V-VI, and in the rest of Russia - up to IV-V degrees, as well as in several countries of Europe, Asia and North America. Macroseismic manifestations of the May 24, 2013 earthquake have been reported at epicentral distances up to 9500 km.

| № | \multicolumn{5}{Hypocenter} | | | | | \multicolumn{7}{Energy class / Magnitudes} | | | | | | |
| | Date YYYY.MM DD. | Time hh:mm:ss | $\phi°$,N | $\lambda°$,E | h, km | KB GS RAS | | | Global CMT | NEIC(USGS) | | Obninsk | |
						K^{F68}	ML	M_c	M_W	m_b	M_W	m_b	M_S
Strong earthquakes of this area for the period from 1962 to May 24, 2013
1	1965.08.01	16:41:07	52.65	152.58	460	14.1	6.3	—	—	5.1	—	—	—
2	1971.01.29	21:57:51	50.19	151.86	710	15.2	7.3	—	—	6.1	—	6.8	—
3	1972.05.27	04:06:45	55.05	156.05	467	14.0	6.2	—	—	5.7	—	6.2	—
4	1975.12.21	10:54:06	50.60	152.61	701	15.2	6.8	—	—	6.0	—	6.4	—
5	1977.09.21	21:01:42	51.32	155.51	247	13.7	6.1	—	—	5.6	—	6.1	—
6	1979.12.30	04:18:21	51.39	152.84	682	13.6	6.0	—	—	5.4	—	5.8	5.0
7	2001.02.07	15:16:10	52.28	153.66	476	14.2	6.4	5.0	5.7	5.6	5.7	5.9	—
8	2008.07.05	02:12:06	53.82	153.53	610	15.7	7.1	6.9	7.7	6.8	7.7	6.9	6.5
9	2008.11.24	09:02:52	53.76	154.69	564	15.2	6.8	6.7	7.3	6.5	7.3	6.5	6.2
10	2009.12.10	02:30:51	53.40	152.61	621	14.8	6.6	5.4	6.3	6.1	6.3	6.2	—
The May 24, 2013 earthquake and its strongest aftershocks
11	2013.05.24	05:44:47	54.76	153.79	630	17.0	7.8	7.4	8.3	7.5	8.3	7.7	—
12	2013.05.24	14:56:29	52.11	151.81	642	15.0	6.8	5.8	6.7	6.7	6.7	7.0	—
13	2013.10.01	03:38:19	52.99	153.25	605	15.2	6.9	6.1	6.7	—	—	6.7	—

Note: K^{F68} - K-class magnitude of S-wave; ML - local magnitude; M_c - coda magnitude; Mw - moment magnitude; m_b - short-period body-wave magnitude; M_S - surface-wave magnitude.

Table 1.1: *Parameters of strong earthquakes ($ML \geq 6.0$) in the Sea of Okhotsk region from 1962 to May 2013, including the May 24, 2013 earthquake and its strongest aftershocks.*

According to the SS TWS regulations real-time data processing started when an alarm signal was released (i.e. when the amplitude on a station exceeds the predetermined threshold value) after registering the P-wave onset at the "Karymshina" station (KRM). Processing was carried out within accepted time limits despite the strong ground shaking with intensities up to IV-V at the office's location. A preliminary assessment of source parameters was obtained within 4 minutes since the alarm, and a final one was released within 8 minutes since the alarm. All the relevant messages were sent according to the circulation list. The on-duty staff decided not to issue a tsunami alarm because the earthquake hypocenter was located at a depth greater than 600 km.

The reference magnitude to assess the tsunamigenic potential of an earthquake in the SS TWS is the
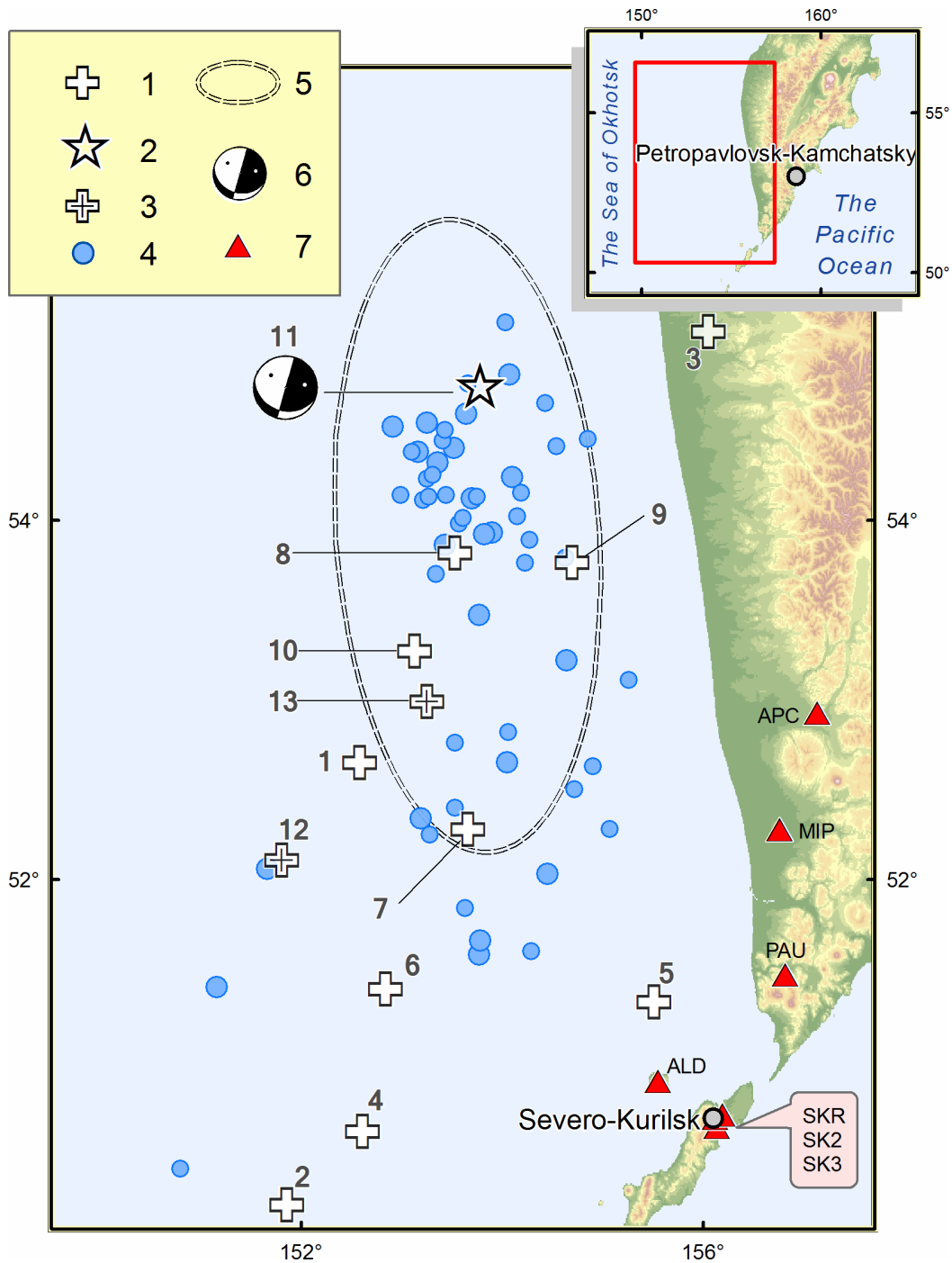
Figure 1.1: *Location scheme for epicenters of the May 24, 2013 earthquake, its aftershocks with magnitudes of $ML \geq 4.2$ and strong earthquakes ($ML > 6.0$) of this region for the period from 1962 to May 24, 2013 according to the catalogue of Kamchatka and the Commander Islands earthquakes ($ML \geq 4.2$ corresponds to the catalogue completeness threshold for the Kamchatka regional network in the Sea of Okhotsk region): 1 -epicenters of strong earthquakes ($ML > 6.0$) of this region for the period from 1962 to May 24, 2013, 2 - the epicenter of the May 24, 2013 earthquake; 3 - epicenters of strong aftershocks ($ML > 6.0$); 4 - epicenters of aftershocks with $4.2 \leq ML \leq 6.0$; 5 - 2σ-ellipse approximation of the aftershock zone; 6 - stereogram of the focal mechanism by Global CMT for the main shock; 7 - seismic stations. Numeration of earthquakes corresponds to Table 1.1.*
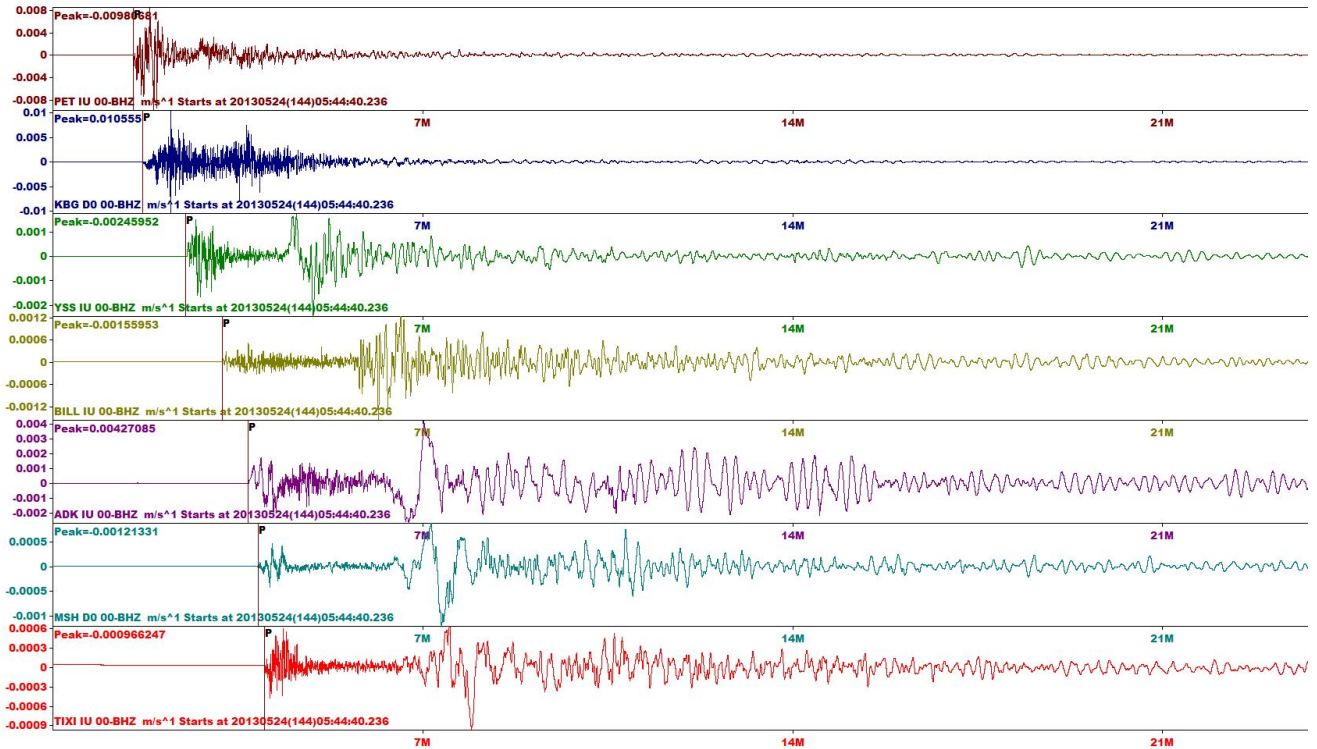
Figure 1.2: *Examples of earthquake records of the May 24, 2013 earthquake at broadband seismic stations (vertical channels): PET - "Petropavlovsk"; KBG - "Krutoberegovo"; YSS - "Yuzhno-Sahalinsk"; BILL - "Bilibino"; ADK - "Adyak"; MSH - "Schultz Cape"; TIXI - "Tiksi"*

surface-wave magnitude M_S. It should be noted that this magnitude has been underestimated in the preliminary solution (M_S=6.7). It is well known that deep earthquakes produce significantly reduced surface waves what leads to magnitude underestimation. Earthquake records are shown in Figure 1.2.

Thus, the earthquake processing time of SS TWS is about 8 minutes, which is within the approved time limit (according to current regulations it should take not more than 10 minutes for processing earthquakes at epicentral distances of up to 1000 km). The processing centre "Petropavlovsk" in a challenging situation demonstrated sufficient accuracy in determination of earthquake parameters within their mission as an urgent service of tsunami warning system.

1.1.2 Tectonic setting and the focal mechanism of the earthquake

The Kuril-Kamchatka subduction zone can be divided along strike into two segments: the Kurile-South-Kamchatsky and the North-Kamchatsky segment (*Levina et al.*, 2013). The boundary between them is located in the Avacha Gulf area. Numerous geological and seismological data confirm the difference in ages of subduction on these two segments. The observed seismic focal zones are characterized in the southern and northern segments by fundamentally different depths, 650–700 km to the south and only 350–400 km to the north, respectively (Figure 1.3).

The deep-focus May 24, 2013 earthquake occurred almost at this boundary, or to be more specific at the north-eastern end of the Kuril-South-Kamchatka segment of the subducting Pacific plate. NE of the epicenter, the depth position of the lower boundary of the Benioff zone moves up, from about 400 km at latitude 53.5°N to about 120 km at 56°N.
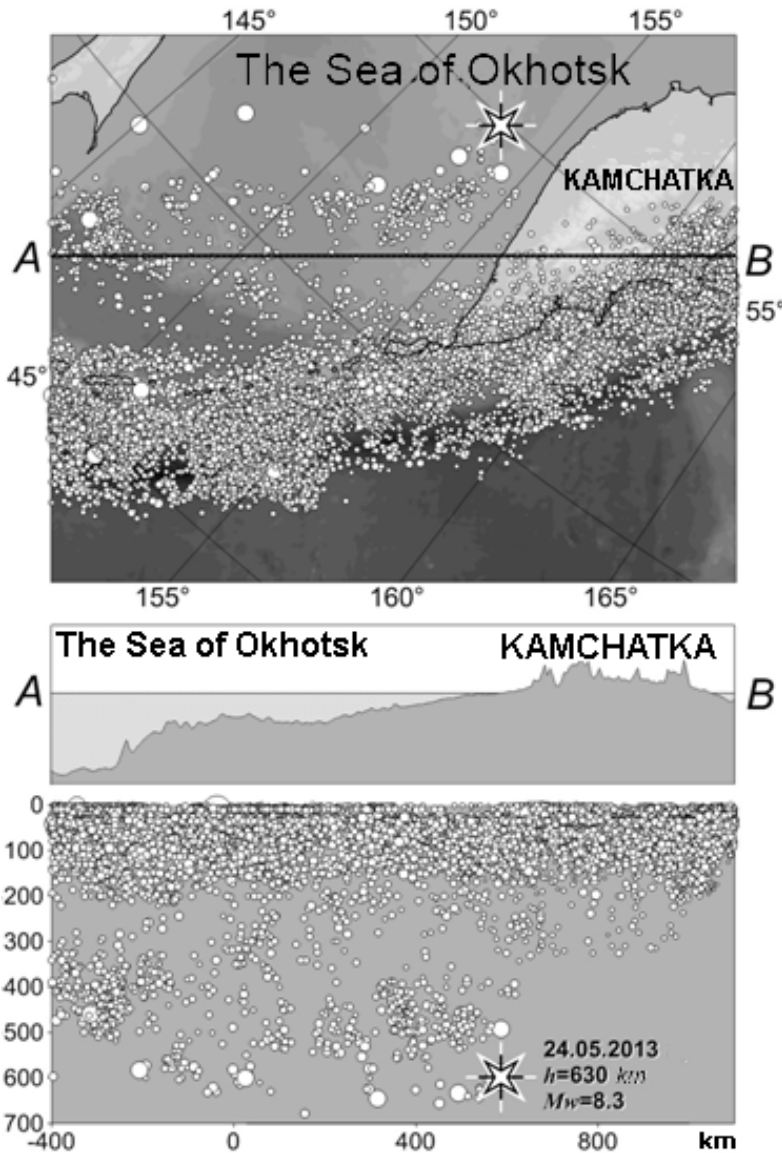
Figure 1.3: *Locations for the epicenters of the May 24, 2013 earthquake and other events of the focal zone from 1962 to August 2013 according to USGS NEIC PDE catalogue and the projection of its hypocenters on the vertical plane along a profile (AB).*

Focal mechanisms were determined using three types of data: (1) polarities of P waves; (2) co-seismic offsets at the GNSS stations (static case); and (3) waveforms registered at regional broadband seismic stations (dynamic case).

Parameters and stereograms of focal mechanisms for the May 24, 2013 earthquake and its strongest aftershocks with $ML \geq 6.0$ according to catalogues of Global CMT and KB GS RAS (the latter estimates are determined using P wave polarities at regional and global stations) are given in Table 1.2. The most interesting fact is that all the solutions indicate compression down dip of the subducting Pacific plate.

The determination of focal mechanism in a general approach as a full seismic moment tensor (SMT) is described in *Abubakirov et al.* (2015), where six SMT components are calculated. The seismic moment tensor was determined using either co-seismic static offsets or waveforms (displacements) by a least-square linear inversion providing error estimations for each of the SMT components as standard deviations. Then the SMT eigenvalues and corresponding principal axes were estimated which allowed to determine (1) the best double couple (DC), (2) scalar seismic moment, $M_0 = (E3 - E1)/2$, and (3) Lode-Nadai coefficient, $\eta = (2E_2 - E_1 - E_3)/(E_3 - E_1)$, where $E_1 \leq E_2 \leq E_3$ are SMT eigenvalues.

№	Date YYYY.MM.DD	Time hh:mm:ss	h, km	The axes of the principal stresses						Nodal planes						Agency	
				T		N		P		NP1			NP2				
				pl	azm	pl	azm	pl	azm	stk	dip	slip	stk	dip	slip		
11	2013.05.24	05:45:08	611	34	102	1	192	56	283	12	79	-89	189	11	-93	Global CMT	
		05:44:47	630	39	81	28	196	39	311	196	90	62	106	28	180	KB GS RAS1)	
12	2013.05.24	14:56:34	642	19	124	11	30	68	272	25	64	-102	231	28	-67	Global CMT	
		14:56:29	642	9	138	9	229	78	3	56	55	-79	218	37	-105	KB GS RAS1)	
13	2013.10.01	03:38:24	585	13	171	28	74	59	284	59	64	-121	293	40	-44	Global CMT	
		03:38:19	605	25	190	21	90	56	325	83	73	-112	318	28	-39	KB GS RAS1)	

Note: 1) Input data are polarities of P-waves.

Table 1.2: *Parameters of focal mechanisms of the May 24, 2013 earthquake and its strongest aftershocks with ML ≥ 6.0 from Table 1.1 according to the Global CMT and KB GS RAS data.*

The η value varies from -1 to 1 ($\eta = 0$ corresponds to the pure double-couple source) and characterizes a discrepancy between a SMT solution and a DC.

In addition to the SMT, in the dynamic case the source is characterized by its source time function (STF), which describes the slip rate. In this study we assume the STF to be an isosceles triangle of unit area and the source epicenter is known from USGS PDE catalogue. The duration of the STF and the source depth are found by best fit during the inversion process.

All calculated variables are accompanied by error estimates. For variables that are functions of SMT components error estimates are obtained by the Monte-Carlo method. Namely, each optimal SMT component is disturbed by random normally distributed quantities with zero mean and standard deviation obtained by the LS inversion. For N realizations (N = 1000) of the SMT, the set of values of a dependent scalar quality, say the largest eigenvalue, is generated. The estimate for such scalar quantity is the half-width of the interval (centered at the undisturbed value) that contains 68% of the points. Note that if a data distribution is normal then 68% of the data values are within one standard deviation of the mean. When we deal with a vector, we find half the angle at the vertex of a circular cone that contains 68% of the vectors based on the disturbed tensors. The axis of the cone is determined by the undisturbed vector.

For the static case we used three-component data from GNSS observations carried out by KB GS RAS and networks of other institutions of the Far Eastern Branch of the Russian Academy of Sciences (Figure 1.4 shows horizontal offsets vectors). We assume that the source is a point source and located at the GCMT centroid. For SMT inversion we used the functions of influence of the SMT components or partial derivatives of Green's functions with respect of source spatial coordinates. The influence functions - synthetic static displacements from unit couple corresponding to each of SMT component - were calculated for a layered sphere using an original algorithm (*Abubakirov et al.*, 2015).
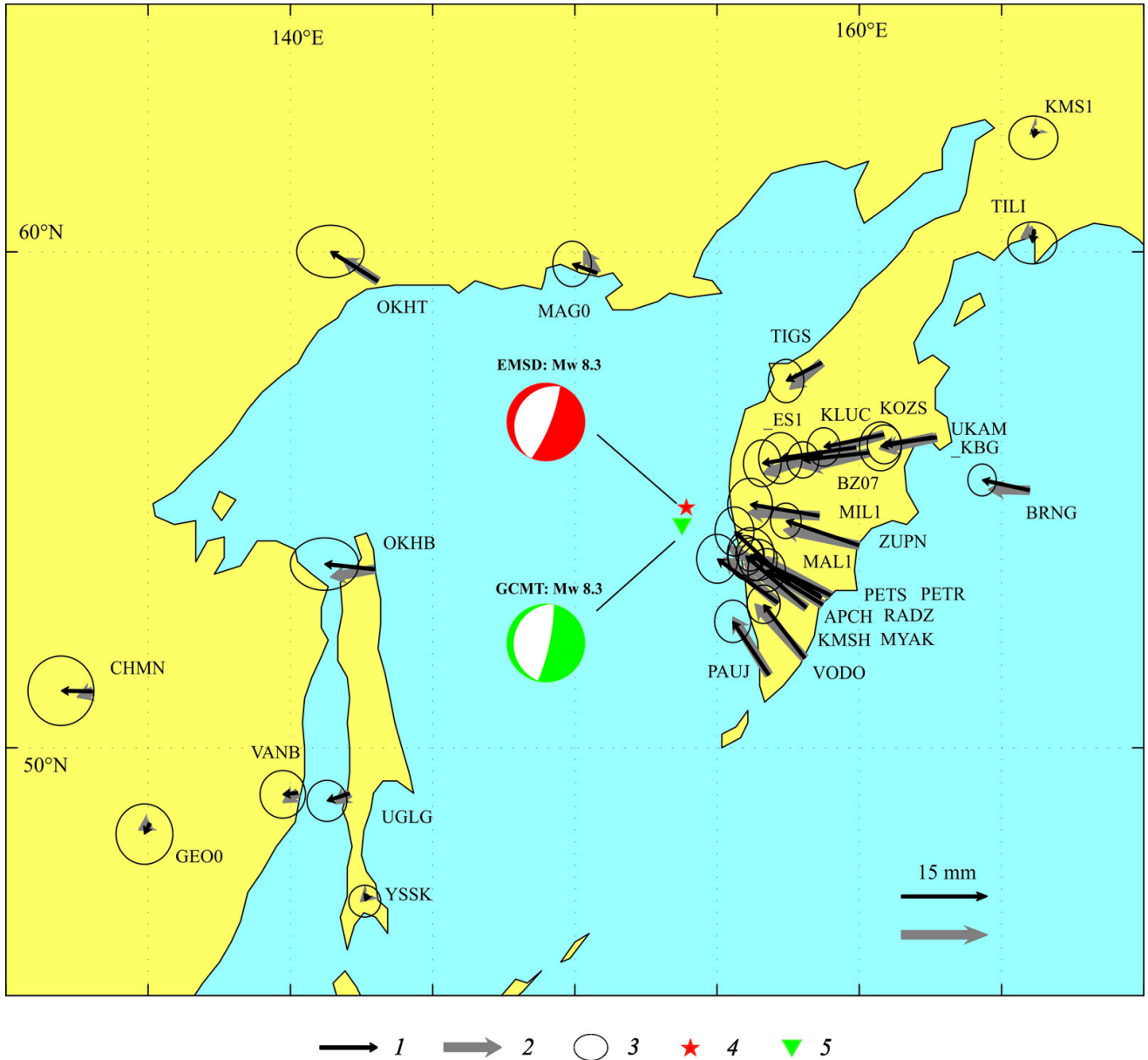
Figure 1.4: *Horizontal components of observed offsets and simulated static displacements for the ES_1 option (parameters used for calculation are given in Table 1.3). 1 - observed horizontal offsets; 2 - simulated static offsets; 3 - error ellipses; 4 - epicenter as located by the KB GS (EMSD); 5 - epicenter according to the GCMT.*

For the dynamic case we used seismic broadband seismograms (Figure 1.5). Four seismic networks were used for processing: GSN (global seismic network), Japanese F-net network, Alaska Regional Network and China National Seismic Network. Additionally, we used reference stations of SS TWS by KB GS RAS and Tsunami Warning Center of USA West Coast and Alaska (West Coast & Alaska Tsunami Warning Center). For the SMT inversion we used records of stations with a low-frequency corner in the velocity transfer function at frequencies less than 8.33 mHz (period of at least 120 s). This condition allows us to reconstruct long-period ground motion with a sufficient enough signal-noise ratio.

The algorithm of dynamic inversion is presented in *Pavlov and Abubakirov* (2012). The functions of influence for the dynamic case were calculated for a layered half-space using the algorithm described in *Pavlov* (2013).

Seismic stations were selected in the epicentral distances of 8–25°. The upper limit of this range is set to ensure the applicability of the flat layered model of media used for the inversion, and the lower one is to ensure far-field conditions as calculations are based on a point-source model.

Calculation cases are described in Table 1.3. Besides the input data type (static or dynamic), they vary by number of components used and/or the number of unknown SMT components.

Used paramters	ES_1	ES14	ES35	ES25	ES35	ES36
Input data	Co-seismic offsets	Co-seismic offsets	Co-seismic offsets	Co-seismic offsets	Wave forms[1]	Wave forms[2]
Method of static offsets evaluation	1-1[3]	14-14[4]	14-14[4]	14-14[4]	-	-
Number of SMT components	3	3	3	2[5]	3	3
Number of unknowns	6	6	5[6]	5	5	6

Note:

1) In the interval $[t_P, t_P + 900]$ s;

2) in the interval $[t_P, t_S]$ s;

3) difference of observations after and before the earthquake;

4) difference of observations based on linear interpolations of data for 2 weeks after and 2 weeks before the earthquake;

5) horizontal components only;

6) SMT is assumed to have zero trace ($M_{11} + M_{22} + M_{33} = 0$).

Table 1.3: *Codes of calculation cases*

The inversion results (Table 1.4, Table 1.5 and Figure 1.6) are compared to three SMT solutions available on the website of the USGS. All of these cases use the same condition (SMT is assumed to have zero trace). In the tables SMT solutions are coded as follows:

USGSW - The W-phase is used as raw data (seismogram segments from direct P wave to surface wave onsets) at regional and teleseismic distances, with filtering in a period range of 100-1000 s;

GCMT - the global catalogue of centroids and moment tensors. For calculations broadband seismograms are used at epicentral distances of ~30° to ~90°. In this case, the body waves are used (with periods of > 50 s) and the mantle waves (with periods of > 200 s);
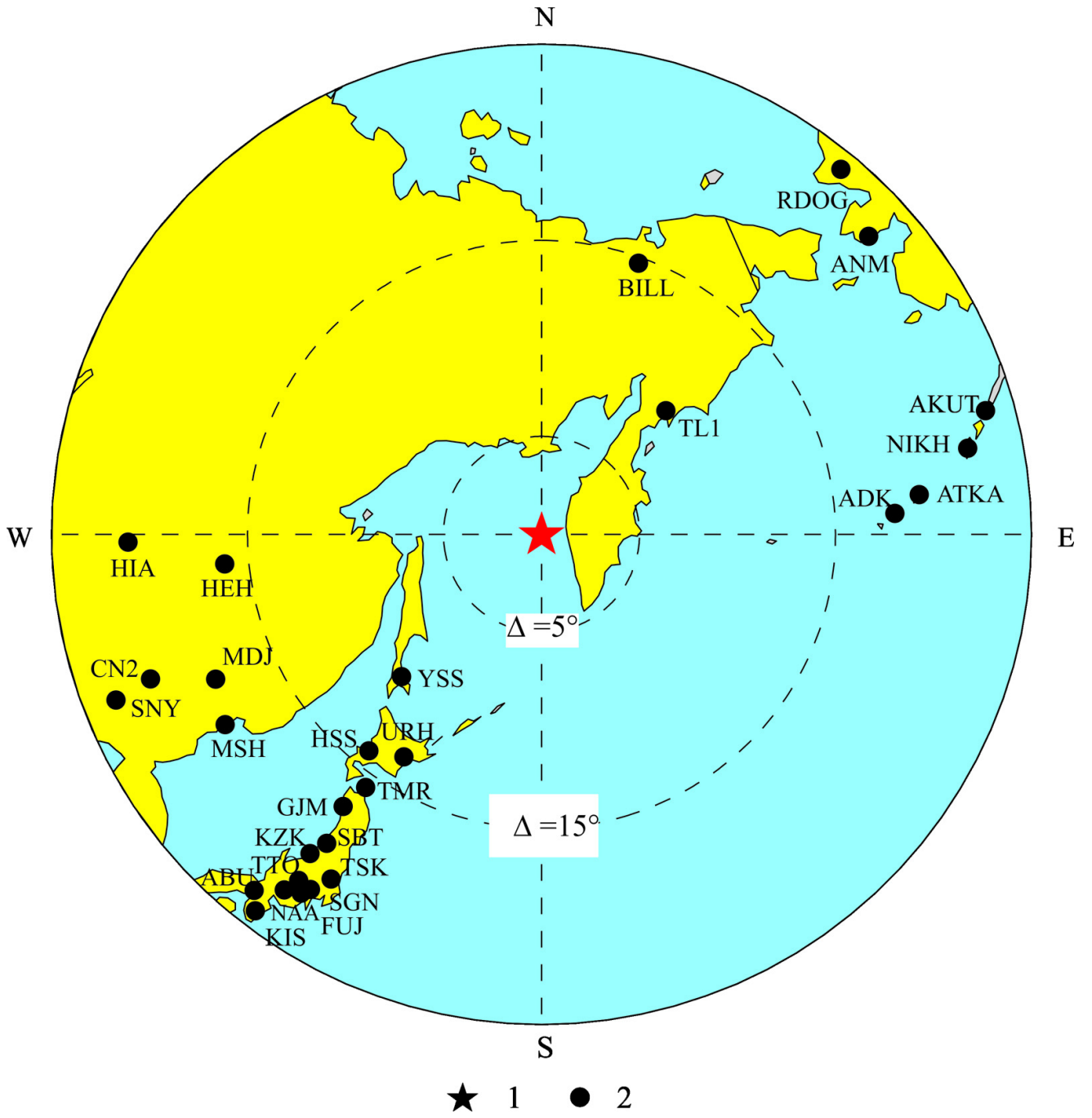
Figure 1.5: *The location of instrumental epicenter by USGS (Table 1.2), the Sea of Okhotsk earthquake on May 24, 2013 (1) and used seismic stations (2).*

Code	M_{11}	M_{12}	M_{13}	M_{22}	M_{23}	M_{33}	ξ	ε, %
	$10^{21} N{\cdot}m$							
GCMT[1]	1.28 ±0.01	-0.16 ±0.01	-3.57 ±0.01	0.38 ±0.01	0.78 ±0.01	-1.67 ±0.01	-	-
ES_1	1.11 ±0.91	-0.52 ±0.36	-3.37 ±0.24	0.27 ±1.19	1.29 ±0.19	-2.48 ±0.46	-0.37 ±0.52	2.6
ES14	1.41 ±0.96	-0.66 ±0.39	-3.71 ±0.24	1.86 ±1.34	1.46 ±0.21	-0.85 ±0.51	0.81 ±0.57	3.7
ES35	0.57 ±0.42	-0.51 ±0.36	-3.74 ±0.24	0.62 ±0.44	1.47 ±0.21	-1.19 -	-	3.8
ES25	0.58 ±0.42	-0.59 ±0.35	-3.84 ±0.24	0. 57 ±0.44	1.60 ±0.22	-1.15 -	-	2.6
ED35	0. 87 ±0.07	-0.06 ±0.07	-3.77 ±0.09	0.41 ±0.07	1.13 ±0.07	-1.29 -	-	20.8
ED36	0. 62 ±0.20	-0.22 ±0.22	-5.06 ±0.37	0.46 ±0.28	1.52 ±0.33	-1.24 ±0.60	-0.06 ±0.23	20.8

Note: 1) It is given in full format (rounded) from GCMT catalogue (rounded).

Table 1.4: *CMT-components M_{ij}, values of isotropic part ξ and residuals ε.*

USGSC - a version of CMT by National Information Center (NEIC) of US Geological Survey. Medium- and long-period body and surface waves were used for the calculations.

Table 1.4 shows the SMT components obtained by inversions and error estimates by the least-squares method. For cases of USGSW and USGSC error estimates are not provided. Also this table shows the values of the isotropic part of the SMT, if it is not assumed to be equal to zero. Table 1.5 shows such calculated variables as: SMT eigenvalues, strike, dip, slip, scalar seismic moment M_0 for the best double couple (DC), discrepancy between SMT solution from DC - η, and also the value of moment magnitude Mw. All these values are given with error estimates. For cases of USGSW and USGSC error estimates are not available.

The duration of rupture process was estimated as 32 seconds. The calculation also gives an independent estimate of the depth, h=640 km, which allowed to estimate the error of about ±50 km. This estimate is consistent with other definitions given in Table 1.2. The duration value is consistent with the independent evaluation of ∼30 s from the work of *Ye et al.* (2013). The value of the duration in the GCMT catalogue is $\tau = 71.4$ s, which is more than double our estimate. However, the GCMT estimate is not a result of direct fitting, but assigned by the magnitude using a correlation equation (*Ekström et al.*, 2012).

For the ES_1 case (using co-seismic offsets, details are in Table 1.3) Figure 1.6 shows the focal mechanism, cones, characterizing error estimates, eigenvectors positions and the neutral axis and quantities for other cases of this study and those obtained by other agencies. All cases show similar solutions.

The M_0 values for all the cases are consistent. The only exception is the ED36 dynamic case. Input data used for ED36 (excluding S waves) are not sufficient enough.

Using seismological data parameters of the finite source, such as rupture velocity (V_r), duration time, rupture area were estimated by *Ye et al.* (2013). They found that the radiated seismic energy E_R is $E_R = 1.5 \times 10^{17}$ J, rupture velocity is $V_r = 4$ km/s, and average stress drop is $\Delta\sigma = 15$ MPa. The

| Code | Eigenvalues, $10^{21} N{\cdot}m$ | | | Focal mechanism | | | η, % | M_0 | M_W |
| | | | | Planes[1] | | Rake[2] | | $10^{21} Nm$ | |
	E_1	E_2	E_3	φ (°)	δ(°)	λs (°)			
USGSW[3]	-4.00	0.31	3.67	12/184	81/10	-89/-98	12	3.84	8.3
GCMT	-4.13 ±0.01	0.36 ±0.01	3.76 ±0.01	12/189 ±0.1/1	79/11 ±0.1	-89/-93 ±0.2/1	14±0.3	3.96 ±0.01	8.331 ±0.001
USGSC[4]	-4.58	0.40	4.18	15/177	81/10	-87/-107	14	4.40	8.4
ES_1	-4.65 ±0.45	0.02 ±1.0	3.52 ±0.66	22/207 ±4/33	76/14 ±3/4	-91/-84 ±8/29	14±24	4.09 ±0.31	8.34 ±0.02
ES14	-3.71 ±0.51	1.30 ±1.07	4.84 ±0.67	25/246 ±5/33	80/13 ±4/5	-98/-50 ±9/27	17±22	4.27 ±0.31	8.35 ±0.02
ES35	-4.30 ±0.37	0.25 ±0.44	4.05 ±0.31	23/238 ±3/26	83/9 ±3/4	-95/-55 ±5/26	9±16	4.17 ±0.26	8.35 ±0.02
ES25	-4.39 ±0.36	0.14 ±0.44	4.25 ±0.32	24/240 ±3/25	83/9 ±3/4	-95/-53 ±4/25	5±15	4.32 ±0.26	8.36 ±0.02
ED35	-4.29 ±0.09	0.42 ±0.07	3.87 ±0.09	16/188 ±1/7	82/8 ±1/1	-89/-98 ±1/7	15±3	4.08 ±0.08	8.34 ±0.01
ED36	-5.64 ±0.51	0.35 ±0.29	5.12 ±0.45	17/213 ±4/22	85/5 ±2/2	-91/-74 ±2/22	11±8	5.38 ±0.37	8.42 ±0.02

Note:

1) The plane orientation is defined by two angles - the strike φ and dip δ (angle for the second plane is given after the slash);

2) Rake λs - the angle in the focal plane between the strike direction and the slip vector (measured anti clockwise from the strike direction);

3) Obtained by W-phase (`http://earthquake.usgs.gov/earthquakes/eventpage/usb000h4jh#moment-tensor?source=us&code=usb000h4jh_Mww`);

4) CMT obtained by USGS NEIC (`http://earthquake.usgs.gov/earthquakes/eventpage/usb000h4jh#moment-tensor?source=us&code=pde20130524054448980_598_C_UCMT`)

Table 1.5: *Parameters of the Sea of Okhotsk earthquake: eigenvalues, mechanism, discrepancy between SMT solution and double couple η, scalar seismic moment M_0, and moment magnitude Mw.*

estimated slip distribution along the fault plane is heterogeneous, with an average slip of 1.9-2.3 m, and a maximum slip of 9.9 m. The rupture area is 180×60 km.

Another interpretation of GNSS data for the Sea of Okhotsk earthquake in terms of a dislocation model are described in *Steblov et al.* (2014) and *Shestakov et al.* (2014), using the shallow dipping plane of the GCMT focal mechanism. Shestakov's input data set is similar to ours; Steblov's data set is not as dense for the Kamchatka part as the other two sets, but includes additional GNSS stations in the Kuril Islands. All three working groups use different methods to determine static offsets from raw data.

The individual determination of such values as fault area (A) and slip (D), instead of A·D, is a challenging task as mentioned in *Steblov et al.* (2014). When the second plane, instead of the preferred one, of the GCMT focal mechanism is used for inversion, a similar misfit is found (*Shestakov et al.*, 2014). In general, observed data are not sufficient to distinguish the true plane orientation; with available GNSS data for this deep-focus earthquake, the only values confidently determined are parameters characterizing an equivalent point source. In other words, due to the focal depth and station network configuration, all the GNSS stations are in the far-field.

The fault center or the source point is (1) assumed as GCMT centroid (*Shestakov et al.*, 2014), (2) found
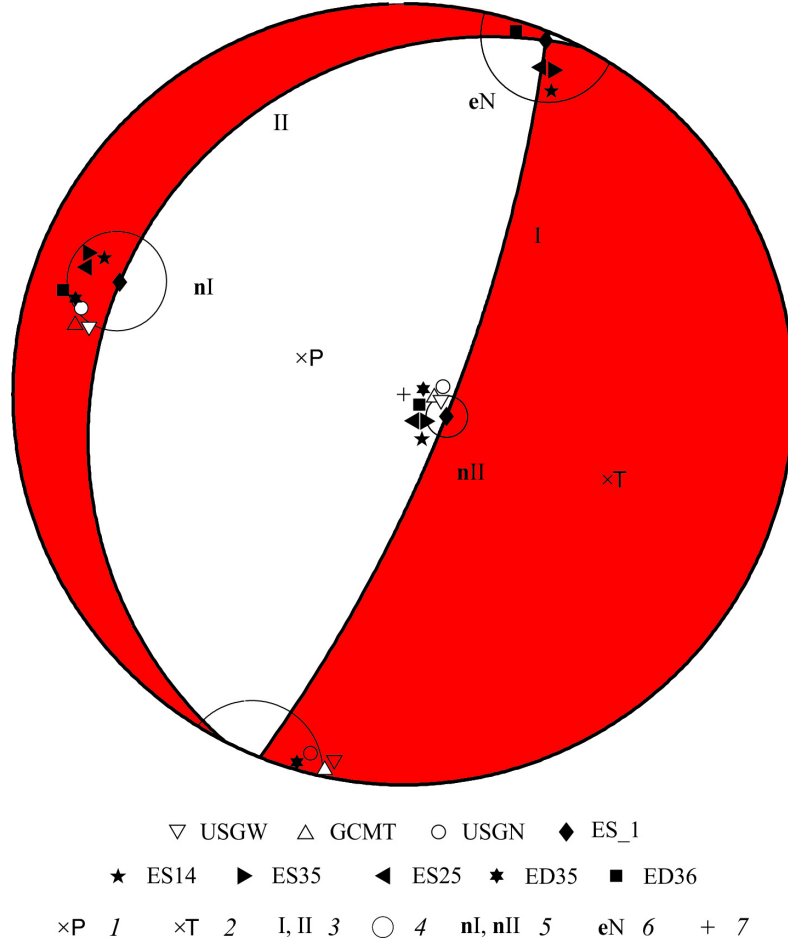
Figure 1.6: *The mechanism for ES_1 case on a stereogram of the lower hemisphere. 1, 2 - axis of stress and strain; 3 - nodal planes; 4 - projection of the part of focal sphere that belongs to a cone reflecting error estimates; eigenvectors position (5) and the neutral axis (6) for all the cases from Table 1.5; 7 - the center of projection. The value of the half-angle of the axial section of the cone equals to 6° for the cone at nI, 9° - at nII and 10° - at eN.*

for the best solution as about 60 km southeast from the GCMT centroid (*Steblov et al.*, 2014), or (3) assumed as NEIC PDE coordinates of the epicenter for the dynamic case and GCMT centroid for the static case (*Abubakirov et al.*, 2015); while the M_0 values are consistent: (1) $M_0 = 4.69 \cdot 10^{21} N \cdot m$, (2) $M_0 = 4.25 \cdot 10^{21} N \cdot m$, and (3) $M_0 = (4.08 - 4.32 \pm 0.31) \cdot 10^{21} N \cdot m$, respectively.

1.1.3 Main features of the aftershock sequence

The aftershock sequence of the May 24, 2013 earthquake, Mw=8.3, consists of 94 earthquakes with magnitudes in the range of ML=3.8-6.9. By its cumulative frequency-magnitude plot (Figure 1.7) the catalogue completeness threshold can be determined as ML=4.2, which corresponds to the left edge of the linear part of the curve. For further analysis 62 earthquakes that occurred prior to April 2014 were selected from the preliminary catalogue based on this threshold.

Figure 1.1 shows an ellipse containing 90% of the aftershocks for the first 14 hours after the major earthquake, allowing to estimate the rupture area of the May 24, 2013 earthquake, Mw=8.3 as 400 km (length)×180 km (width).
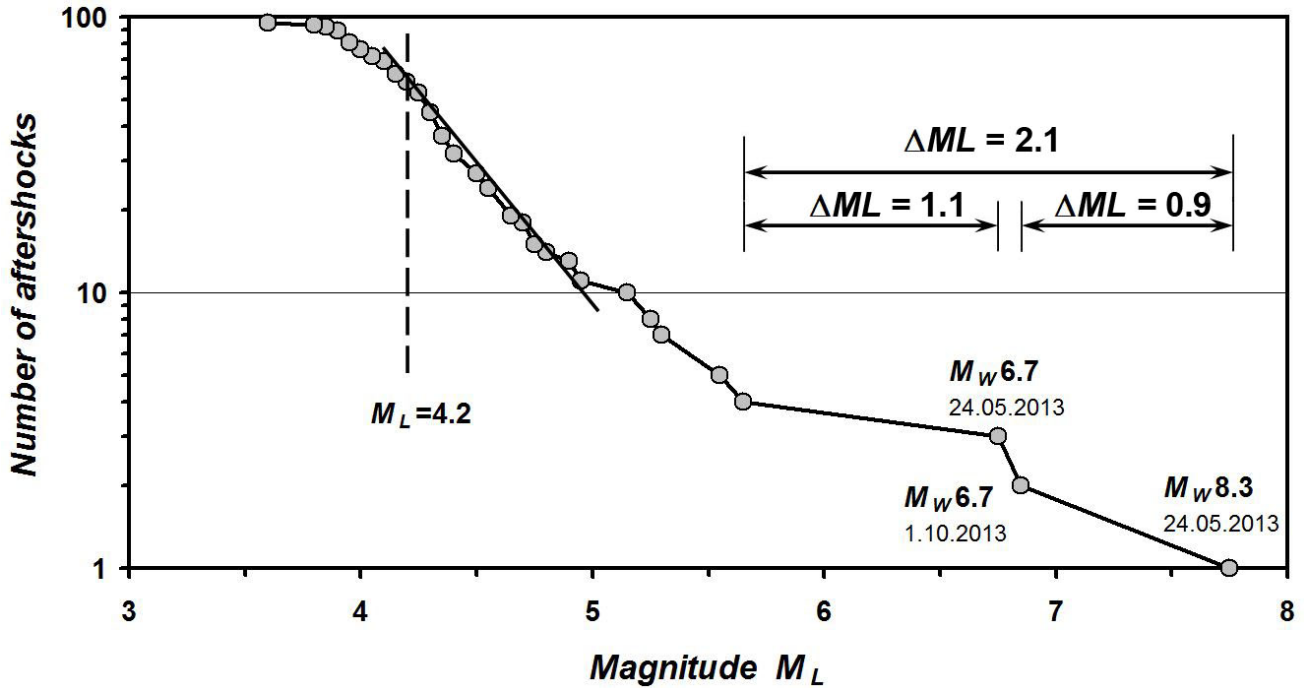
Figure 1.7: *Cumulative frequency-magnitude plot for the aftershocks sequence of the May 24, 2013 earthquake with Mw=8.3.*

According to the frequency-magnitude plot (Figure 1.7) the energy interval between the main event and the strongest aftershock ΔML=0.9 is comparable to the interval between the two strongest aftershocks and a relatively numerous group of aftershocks with a continuous energy distribution (ΔML=1.1).

Figure 1.8 shows the cumulative number of aftershocks over time in logarithmic time scale. The aftershock sequence can be divided into several stages based on the change of the slope of the plot.

First of all, it is necessary to exclude the initial stage with a duration of an hour and consisting of 6 aftershocks with magnitudes between ML=4.4–5.3 from consideration because we believe that powerful coda-waves of the main shock could have masked several events.

The remaining sequence of earthquakes can be divided into three stages, each of which is approximated by a straight line on the plot of Figure 1.8 that has a semi-log scale. This approximation corresponds to a hyperbolic decay of dN/dt where the slope of the line is represented by a proportionality coefficient A. Note that the last segment of the hyperbolic-law approximation is less reliable because of the small amount of data.

A peculiar feature is the coincidence of the two stage changes and the two most powerful aftershocks with magnitude Mw=6.7 each: on May 24, 2013 (9 hours after the main shock) and on October 01, 2013 (after >4 months). None of these earthquakes triggered its own aftershock sequence.

It should also be noted that the May 24, 2013 earthquake with Mw=6.7 at the end of the most intense part of the aftershock sequence occurred outside the ellipse containing 90% of aftershocks of the Mw=8.3 earthquake, and it can be alternatively qualified as a separate event, not as an aftershock in a narrow sense (№12 in Figure 1.1).

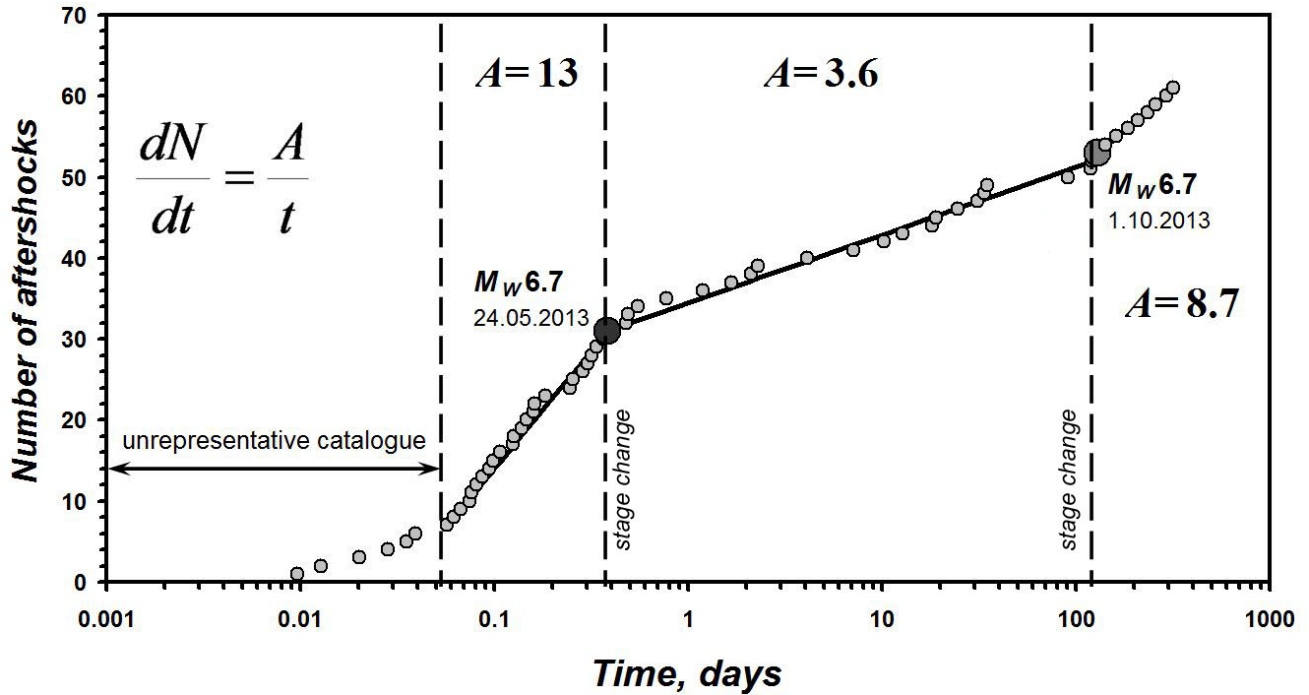**Figure 1.8:** *The typical stages of the aftershock process of the May 24, 2013 earthquake, Mw=8.3. The starting point corresponds to the main event origin. Time bounds of the stages with linear trends are indicated.*

1.1.4 Macroseismic data

Macroseismic information was collected for 190 settlements. From various sources, 546 responses were processed, of which 90 messages of 29 sites were received through the Internet-based questionnaire (http://www.emsd.ru/lsopool/poll.php).

The Sea of Okhotsk earthquake on May 24, 2013 had a great area of macroseismic impact, while it nowhere had any catastrophic manifestations. This event was felt with intensities up to VI degrees on the MSK-64 scale in the settlements located from the epicenter at distances from 139 to 9470 km. In the northern hemisphere of the Earth on a significant part of Eurasia and North America its effect was reported in Russia, Kazakhstan, Japan, China, India, the United Arab Emirates, Poland, Canada, the USA, Mexico, Italy, Estonia and Kyrgyzstan; in the southern hemisphere - in Indonesia on the Java island.

In the Kamchatka area macroseismic data from 64 settlements, were collected. In 50 of them the earthquake was reported to be felt with intensities of II to VI degrees (Figure 1.9). The nearest site to the epicenter, Krutogorovo village, and other towns of the western coast of the Kamchatka Peninsula reported intensities of no more than IV degrees, with the exception of the Oktiabrsky village (I = V degrees). The strongest ground shaking was reported in areas of the eastern coast: I = VI degrees on the Semyachik meteorological station and in the Valley of Geysers, I = V-VI degrees at the Krugly lighthouse. Thus, the highest intensities were reported close to the deep sea trench. This feature is typical for deep island arcs earthquakes, and was first seen in the early 20th century for events in the Benioff zone in Japan (*Utsu*, 1966). It was concluded that this phenomenon was caused by large inhomogeneities within island arcs.

To collect macroseismic information for the Sea of Okhotsk earthquake outside of Kamchatka official
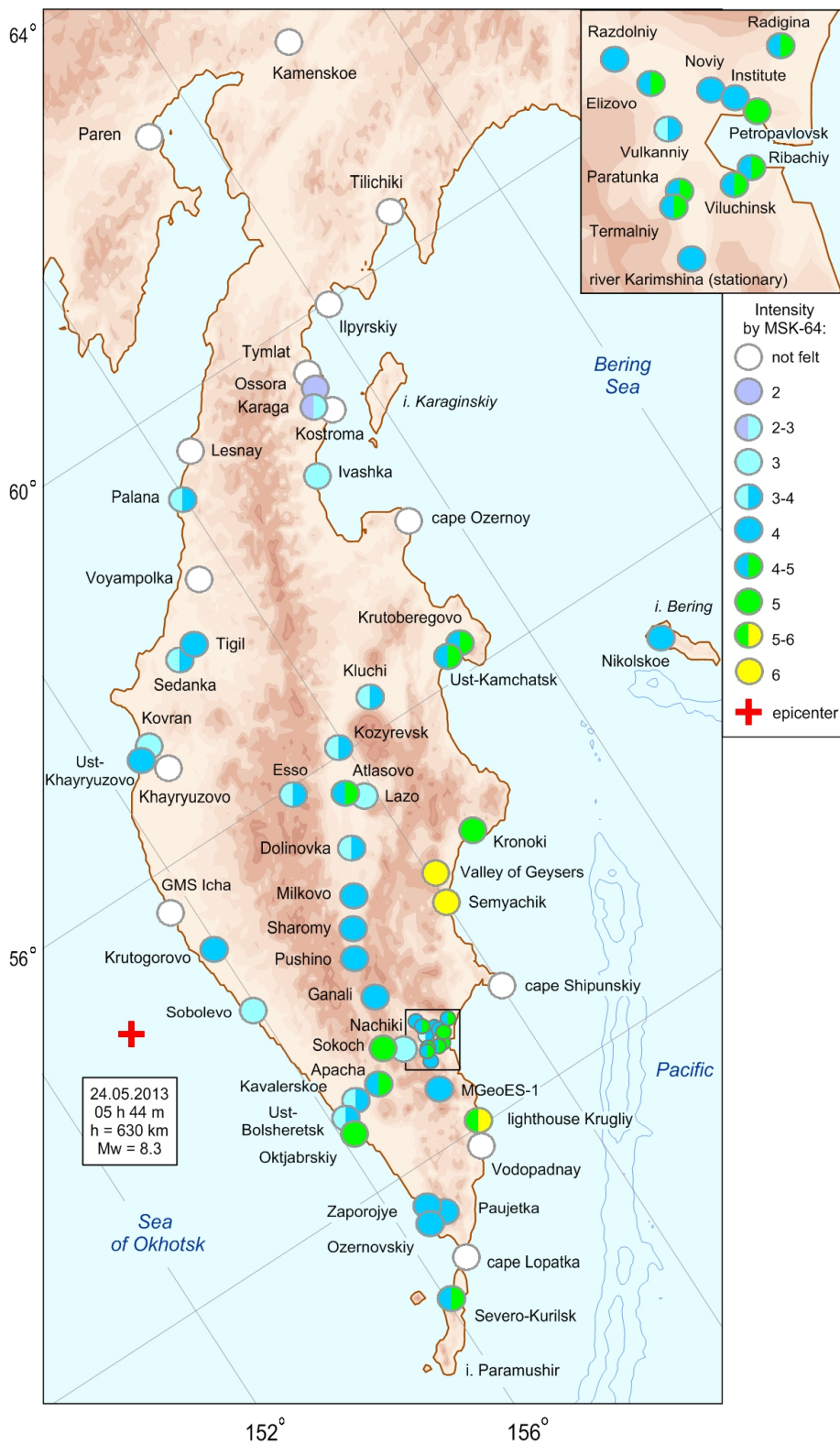
Figure 1.9: *Macroseismic intensity distribution for the Sea of Okhotsk earthquake on May 24, 2013 at the settlements of the Kamchatka region and the Northern Kuriles.*

requests were sent to the Russian Ministry of Emergency Situations, all the Branches of the Geophysical Service RAS and Siberian Branch of the Geophysical Survey RAS, The Schmidt Institute of Physics of the Earth RAS, Mining Institute of the Ural Branch of RAS and other scientific institutions in different regions of Russia. Letters were sent to fellow seismologists from Azerbaijan, Kyrgyzstan, Uzbekistan, Belarus, Moldova, as well as in Kazakhstan National Data Center with a kind request to provide all the available information about the manifestations of this earthquake. There were 17 responses received out of 29 requests sent. The most detailed information was sent by A. D. Zavyalov (IPE RAS), E. P. Semenova (Sakhalin Branch of GS RAS), N. A. Gileva (Baikal Branch of GS RAS), L.I. Karpenko (Magadan Branch of GS RAS), and R.A. Diagilev (Mining Institute of the Ural Branch of RAS, Perm). In addition, information was collected from a variety of news and other Internet resources. We express our sincere gratitude to all those who assisted in the collection of macroseismic data.

As a result, in addition to the Kamchatka region, macroseismic information was obtained from 82 settlements in the territory of Russia, of which 75 reported intensities from II to IV-V degrees. The earthquake was felt by the residents of the Far East (except Primorsky region, Figure 1.10), Siberian, Volga, Central, Southern, North Caucasus and the North-West Federal District (FD) of the Russian Federation.

In Russia, outside Kamchatka, the strongest ground shaking with I = IV-V degrees were reported at two sites: Severo-Kurilsk and Gornoe in the Sakhalin region. Shaking of the intensity of IV was felt in the city of Magadan and Klepka in the Magadan region, Uglegorsk, Aniva, Tymovskoe and Troitskoye in the Sakhalin region. In Moscow and Khabarovsk the earthquake intensity manifestations varied from II to IV, obviously, depending on the soil type and construction quality. In other Russian towns the earthquake was felt with almost equal intensity of about II to III. From Kazakhstan National Data Center macroseismic information was obtained for 7 settlements located on the territory of Kazakhstan, which allowed to specify the data featured at the US Geological Survey (USGS) (http://earthquake.usgs.gov/earthquakes/dyfi/).

According to information received from the Seismological Service of Moldova, Belarus and Azerbaijan, the earthquake in these countries was not felt. On the website of the European Mediterranean Seismological Centre (EMSC) (http://www.emsc-csem.org/Earthquake/Testimonies/comments.php?id=318696) testimonies of the Sea of Okhotsk earthquake from Estonia, Italy, Kyrgyzstan are available. However, intensities are not available.

Figure 1.10 also provides information about macroseismic manifestations in different areas of the world, compiled by the US Geological Survey (USGS) using their DYFI system (Did You Feel It?) (*Wald et al.*, 2011). Texts of received questionnaires were kindly provided to us by the USGS employee, D.J. Wald. The analysis of the text messages received allowed assessing ground shaking intensities at these sites using the MSK-64 scale (*Medvedev et al.*, 1965). In most reports the intensities do not exceed III. Only in the United States there were 2 sites with more notable shaking: the greatest intensity with I = IV-V degrees in Goleta and with I = III-IV degrees in the city of Rock Island, IL.

Thus, macroseismic effects of the 2013 Sea of Okhotsk earthquake were manifested globally. It was felt in almost all major cities of Russia and caused a considerable interest of seismologists. Macroseismic effects of the Sea of Okhotsk earthquake are studied in a number of papers, for example, *Zhigalin et al.* (2013), *Tatevosian et al.* (2014) and others. The most complete descriptions of the macroseismic impact
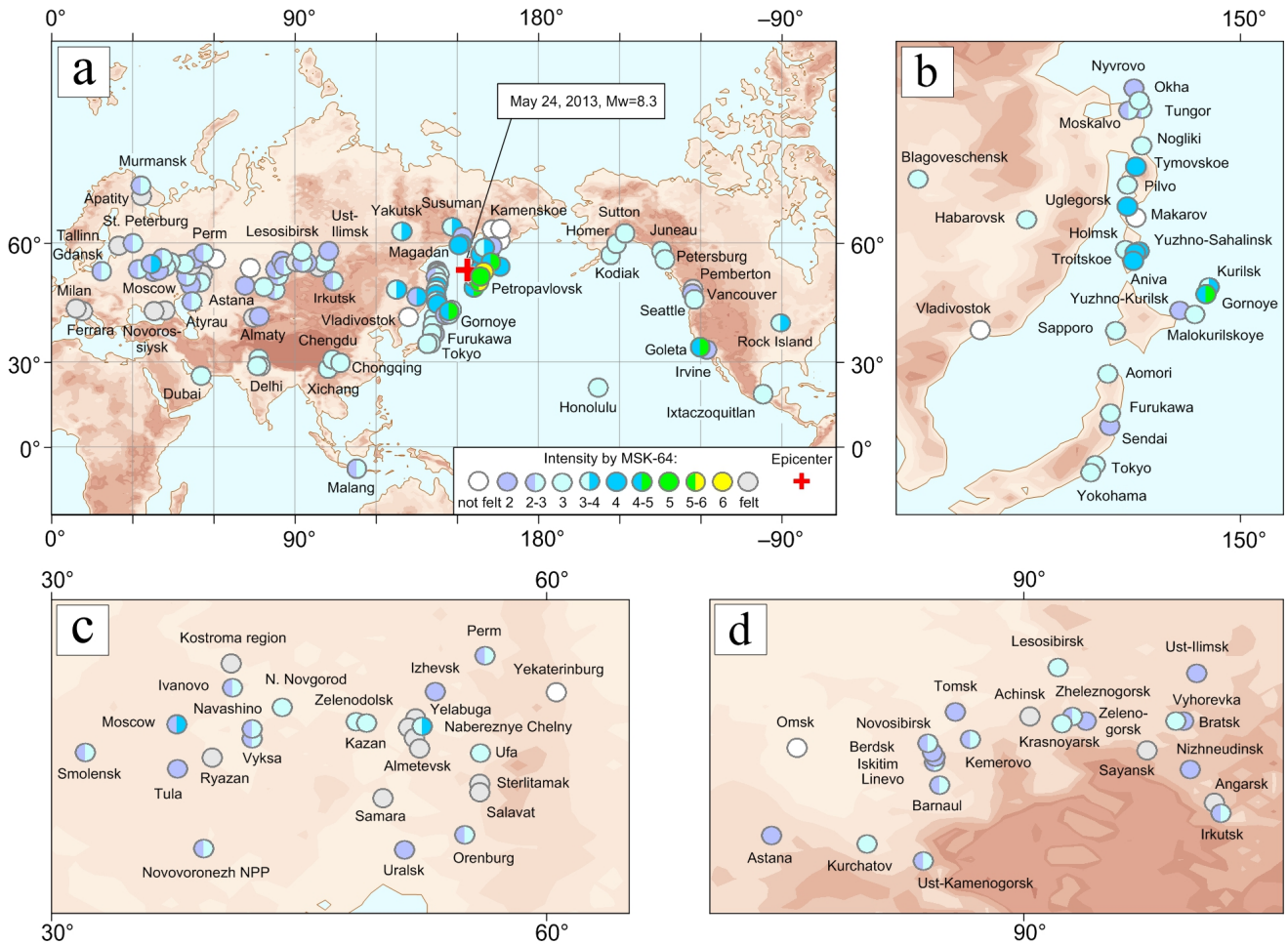
Figure 1.10: *a) Macroseismic map of the Sea of Okhotsk earthquake on May 24, 2013 (MSK-64 intensity scale). More details: b) Japan - Sakhalin - Primorye, epicentral distances, $\Delta = 10\text{-}20^o$; (C) Central Russia - Ural, $\Delta = 50\text{-}60^o$; (G) Siberia - North Kazakhstan, $\Delta = 30\text{-}40^o$.*

worldwide are shown in *Chebrov* (2014) and *Chebrova et al.* (2015).

1.1.5   Conclusion

On May 24, 2013 under the Sea of Okhotsk in the area of responsibility of the Kamchatka regional seismological network, at a depth of 630 km the strongest earthquake recorded in the years of detailed observations (from 1961 to the present time) occurred with a magnitude of Mw=8.3.

The main features of the deep-focus May 24, 2013 earthquake are:

- tectonic setting: the hypocentre is located at the north-eastern end of the Kuril-South-Kamchatka segment of the subducting Pacific plate;

- the main shock as well as the aftershocks are located near the depth limit of earthquake occurrence;

- abnormal range of macroseismic manifestations: the earthquake was felt at teleseismic distances in many settlements of Russia from Kamchatka to the territory of the East European Plain, as well as in countries of Asia (Japan, China, India and others), North America and Pacific;

- co-seismic offsets were observed at the majority of GNSS stations in Far East of Russia.

The parameters of the May 24, 2013 earthquake have been evaluated within 8 minutes from the time of registration of the earthquake within Urgent Message Service and SS TWS, which were sent to the Ministry of Emergency Situations and other relevant agencies.

In the preliminary stage macroseismic information was collected in the Kamchatka area, and the aftershock sequence was processed revealing several stages of the aftershock process.

From the aftershock distribution the rupture area of the May 24, 2013 earthquake is estimated as 400 km (length) $\times$ 180 km (width) with a depth range of 425–720 km.

Estimates of focal mechanisms produced by various methods show similar solutions.

Despite the global macroseismic effect, in nearby settlements (Kamchatka region) the earthquake was felt with intensity of up to V-VI degrees and did not cause any damages.

1.2   References

Abubakirov, I. R., V. M. Pavlov and N. N. Titkov (2015), The mechanism of the deep-focus, Sea of Okhotsk earthquake of May 24, 2013 as inferred from static displacements and broadband seismograms, *Journal of Volcanology and Seismology*, *9*(4), 242-257, DOI:10.1134/S0742046315040028.

Chebrov, V. N., D. V. Droznin, Yu. A. Kugaenko, V. I. Levina, S. L. Senyukov, V. A. Sergeev, Yu. V. Shevchenko and V. V. Yashchuk (2013), The system of detailed seismological observations in Kamchatka in 2011, *Journal of Volcanology and Seismology*, *7*(1), 16–36, DOI:10.1134/S0742046313010028.

Chebrov V. N. (Ed.) (2014): *Strong earthquakes of Kamchatka in 2013*. Petropavlovsk-Kamchatsky: New Book Company, 2014. 252 p. ISBN 978-5-87750-298-7 [In Russian].

Chebrova A. Yu, V. N. Chebrov, A. A. Gusev, A. V. Lander, E. M. Guseva, S. V. Mityushkina and A. A. Raevskaya (2015), The Impacts of the Mw 8.3 Sea of Okhotsk Earthquake of May 24, 2013 in Kamchatka and Worldwide, *Journal of Volcanology and Seismology*, *9*(4), p. 223–241, DOI:10.1134/S074204631504003X.

Ekström, G., M. Nettles and A. M. Dziewonski (2012), The global CMT project 2004-2010: centroid-moment tensors for 13,017 earthquakes, *Phys. Earth Planet. Inter.*, *200*, 1–9, DOI:10.1016/j.pepi.2012.04.002.

Levina, V. I., S. V. Mityushkina, A. V. Lander and A. Yu. Chebrova (2013), The seismicity of the Kamchatka region: 1962-2011, *Journal of Volcanology and Seismology*, *7*(1), 37–57, DOI:10.1134/S0742046313010053.

Medvedev, S. V., V. Shponhoyer and V. Karnik (1965), Scale of seismic intensity MSK-64, *Academy of Science of USSR*, 11.

Pavlov, V. M. and I. R. Abubakirov (2012), Algorithm for calculation of seismic moment tensor of strong earthquakes using regional broadband seismograms of body waves, Bulletin of Kamchatka regional association «Educational-scientific center». *Earth sciences*, *20*(2), 149–158 [in Russian].

Pavlov, V. M. (2013), Algorithm for calculating synthetic seismograms in a layered half-space with application of matrix impedance, *Izvestiya Physics of the Solid Earth*, *49*(1), 24–33, DOI:10.1134/S1069351313010102.

Shestakov, N. V., M. Ohzono, H. Takahashi, M. D. Gerasimenko, V. G. Bykov, E. I. Gordeev, V. N. Chebrov, N. N. Titkov, S. S. Serovetnikov, N. F. Vasilenko, A. S. Prytkov, A. A. Sorokin, M. A. Serov, M. N. Kondratyev and V. V. Pupatenko (2014), Modeling of coseismic crustal movements initiated by the May 24, 2013, Mw=8.3 Okhotsk deep focus earthquake, *Doklady Earth Sciences*, *457*(2), 976–981, DOI:10.1134/S1028334X1408008X.

Steblov, G. M., G. Ekström, M. G. Kogan, J. T. Freymueller, N. N. Titkov, N. F. Vasilenko, M. Nettles, Yu. V. Gabsatarov, A. S. Prytkov, D. I. Frolov and M. N. Kondratyev (2014), First geodetic observations of a deep earthquake: The 2013 Sea of Okhotsk Mw 8.3, 611 km-deep, event, *Geophys. Res. Lett.*, 41, 3826–3832, DOI:10.1002/2014GL060003.

Tatevosian, R. E., G. L. Kosarev, V. V. Bykov, S. A. Maciejewski, I. V. Ulomov, Z. Y. Aptekman and R. N. Vakarchuk (2014), Deep earthquake with Mw=8.3 was felt at a distance of 6500 km, *Izvestiya Physics of the Solid Earth*, 3, 154–162, DOI:10.1134/S1069351314030124.

Utsu, T. (1966), Regional differences in absorption of seismic waves in the upper mantle as inferred from abnormal distributions of seismic intensities, *Geophysics*, *2*(4), 359-374.

Wald, D. J., V. Quitoriano, L. A. Dengler and J. W. Dewey (1999), Utilization of the Internet for rapid community intensity maps, *Seismological Research Letters*, *70*(6), 680–697, DOI:10.1785/gssrl.70.6.680.

Ye, L., T. Lay, H. Kanamori and K. D. Koper (2013), Energy release of the 2013 Mw=8.3 Sea of Okhotsk earthquake and deep slab stress heterogeneity, *Science*, *341*(6152), 1380-1384, DOI:10.1126/science.1242032.

Zhigalin, A. D., A. D. Zav'yalov, I. G. Mindel, A. A. Nikonov, O. G. Popova, E. A. Rogozhin, A. I. Ruzaikin and V. V. Sevost'yanov (2014), The phenomenon of the Sea of Okhotsk Earthquake of May 24, 2013, in Moscow, *Herald of the Russian Academy of Sciences*, *84*(4), 283–291, DOI:10.1134/S1019331614040054.